npj | parkinson's disease

Article

Published in partnership with the Parkinson's Foundation

https://doi.org/10.1038/s41531-024-00707-0

PARKIN is not required to sustain OXPHOS function in adult mammalian tissues

Roberta Filograna[1] ✉, Jule Gerlach[1], Hae-Na Choi[2,3], Giovanni Rigoni[1], Michela Barbaro[4], Mikael Oscarson[4], Seungmin Lee[1], Katarina Tiklova[5], Markus Ringnér[6], Camilla Koolmeister[1], Rolf Wibom[4], Sara Riggare[7], Inger Nennesmo[8], Thomas Perlmann[5], Anna Wredenberg[1,4], Anna Wedell[4,9], Elisa Motori[2,3], Per Svenningsson[10,11] & Nils-Göran Larsson[1] ✉

Loss-of-function variants in the *PRKN* gene encoding the ubiquitin E3 ligase PARKIN cause autosomal recessive early-onset Parkinson's disease (PD). Extensive in vitro and in vivo studies have reported that PARKIN is involved in multiple pathways of mitochondrial quality control, including mitochondrial degradation and biogenesis. However, these findings are surrounded by substantial controversy due to conflicting experimental data. In addition, the existing PARKIN-deficient mouse models have failed to faithfully recapitulate PD phenotypes. Therefore, we have investigated the mitochondrial role of PARKIN during ageing and in response to stress by employing a series of conditional Parkin knockout mice. We report that PARKIN loss does not affect oxidative phosphorylation (OXPHOS) capacity and mitochondrial DNA (mtDNA) levels in the brain, heart, and skeletal muscle of aged mice. We also demonstrate that PARKIN deficiency does not exacerbate the brain defects and the pro-inflammatory phenotype observed in mice carrying high levels of mtDNA mutations. To rule out compensatory mechanisms activated during embryonic development of *Parkin*-deficient mice, we generated a mouse model where loss of PARKIN was induced in adult dopaminergic (DA) neurons. Surprisingly, also these mice did not show motor impairment or neurodegeneration, and no major transcriptional changes were found in isolated midbrain DA neurons. Finally, we report a patient with compound heterozygous *PRKN* pathogenic variants that lacks PARKIN and has developed PD. The PARKIN deficiency did not impair OXPHOS activities or induce mitochondrial pathology in skeletal muscle from the patient. Altogether, our results argue that PARKIN is dispensable for OXPHOS function in adult mammalian tissues.

Pathogenic variants in the *PRKN* gene, also known as *PARK2 or PARKIN*, were identified over twenty-five years ago in patients affected by an autosomal recessive form of PD[1,2]. Comprehensive screens of large PD patient populations have revealed that *PRKN* variants are an important cause of early-onset PD[3,4]. A variety of disease-causing mutations, including single base-pair substitutions, small and large deletions, and splice site variants, have been identified and typically lead to abolished PARKIN expression[5]; almost 50% of variants are copy number variants[6]. Besides homozygosity or compound heterozygosity for several loss-of-function mutations, haplo-insufficiency caused by

[1]Department of Medical Biochemistry and Biophysics, Karolinska Institutet, Stockholm, Sweden. [2]Institute for Biochemistry, University of Cologne, Cologne, Germany. [3]Cologne Excellence Cluster on Cellular Stress Responses in Aging-Associated Diseases (CECAD), University of Cologne, Cologne, Germany. [4]Centre for Inherited Metabolic Diseases, Karolinska University Hospital, Stockholm, Sweden. [5]Department of Cell and Molecular Biology, Karolinska Institutet, Stockholm, Sweden. [6]Department of Biology, National Bioinformatics Infrastructure Sweden, Science for Life Laboratory, Lund University, Lund, Sweden. [7]Department of Women's and Children's Health, Uppsala University, Uppsala, Sweden. [8]Department of Oncology-Pathology, Karolinska Institutet, Stockholm, Sweden. [9]Department of Molecular Medicine and Surgery, Karolinska Institute, Stockholm, Sweden. [10]Department of Clinical Neuroscience, Karolinska Institutet, Stockholm, Sweden. [11]Department of Neurology, Karolinska University Hospital, Stockholm, Sweden. ✉e-mail: roberta.filograna@ki.se; nils-goran.larsson@ki.se

heterozygous *PRKN* variants have been suggested to be risk factors for PD development[7].

PARKIN is a 465 amino acid ubiquitin E3 ligase residing in the cytosol and on the outer mitochondrial membrane (OMM), where it is involved in targeting substrates for degradation through the ubiquitin/proteasome system[8]. Initially, it was hypothesized that loss of PARKIN would result in the accumulation of toxic substrates causing the degeneration of dopaminergic (DA) neurons and eventually PD. Although the function of PARKIN remains controversial, a wealth of data implicates PARKIN in the maintenance of mitochondrial integrity and quality control through the degradation of damaged mitochondria (mitophagy) or the regulation of mitochondrial biogenesis, or by affecting mitochondrial fusion and fission[9].

The consequences of PARKIN loss have been investigated by many research groups using both in vitro and in vivo models. In particular, the involvement of PARKIN in mitophagy has mainly been established by inducing high PARKIN expression in cancer cell lines lacking the endogenous protein. Treatment of these cells with a high concentration of mitochondrial uncoupling agents, e.g., CCCP/FCCP, leads to depolarization of mitochondria and other cellular compartments, including lysosomes, and to the localization of PARKIN to the OMM[10,11]. Although this phenomenon is robustly occurring in cell culture systems, serious concerns have been raised about the in vivo relevance because of the ectopic expression of PARKIN and the non-physiological, near total mitochondrial membrane potential depolarization[12,13].

Elegant studies in *Drosophila melanogaster* have demonstrated that PARKIN plays an important role in mitochondrial maintenance in several tissues, including thoracic flight muscles, DA neurons, and sperm[14,15]. Although PARKIN-deficient fruit flies exhibit enlarged mitochondria with disrupted mitochondrial ultrastructure[15], experiments with pH-sensitive fluorescent mitophagy reporters have failed to unambiguously show that the mitochondrial defects are caused by impaired mitophagy[16,17]. It thus remains unclear whether the flight muscle phenotype in *Parkin*-knockout flies is caused by defective mitophagy, accumulated mitochondrial damage and degeneration, or if it is due to impaired mitochondrial biogenesis during development.

In mice, germline knockout of *Parkin* does not cause DA neuron death or motor deficits[18,19]. However, a modest increase of extracellular DA levels has been reported in the striatum[18] and may possibly constitute a compensatory response. Recent studies have reported that the *Parkin* knockout mice have a minor accumulation of damaged mitochondria in DA neurons[20] and partially impaired oxidative phosphorylation (OXPHOS) in skeletal muscle leading to myofiber atrophy[21]. A plausible explanation for the lack of robust and obvious phenotypes in germline *Parkin* knockout mice is a compensation taking place during development. This hypothesis has been further supported by the DA neuron degeneration observed in conditional knockout mice where loss of *Parkin* is induced in the adult *Substantia nigra*. Furthermore, to generate reliable PD mouse models, germline *Parkin* knockout mice have been crossed to mouse models of mitochondrial dysfunction carrying high levels of mutations[22,23] or double-strand breaks[24] of mtDNA. However, these studies have generated conflicting outcomes, and it remains unclear whether PARKIN loss promotes a more severe pathology.

In this paper, we have performed a series of analyses in the mouse to determine how the absence of PARKIN affects OXPHOS capacity during ageing and upon mitochondrial stress. We have also investigated how *Parkin* disruption in adult DA neurons affects locomotion and transcriptional responses in this neuronal population. Our results do not support an important role for PARKIN in maintenance of the OXPHOS system in the mouse. Lastly, to investigate the relevance of these findings in human pathophysiology, we analyzed a patient with autosomal recessive PD caused by a known and a previously undescribed *PRKN* pathogenic variant that both abolish the expression of PARKIN. In this patient, PARKIN loss did not impair OXPHOS function in skeletal muscle and no signs of mitochondrial myopathy were present.

Results

Mitochondrial function is maintained in aged mice lacking PARKIN

There are several reports that homozygous *Parkin* knockout mice are indistinguishable from controls during their first months of life[25,26,19], but it is unclear whether the age-associated decline in mitochondrial function[27,28] will induce a phenotype. To study the impact of PARKIN loss in aged mice, we generated germline whole-body knockout mice by breeding heterozygous mice with a loxP-flanked exon 7 of *Parkin* (*Parkin*$^{+/loxP}$)[19] to mice ubiquitously expressing cre-recombinase (β-actin-cre). This cross generated heterozygous knockouts (*Parkin*$^{+/-}$) that were intercrossed to obtain homozygous knockouts (*Parkin*$^{-/-}$). The β-actin-cre transgene was removed by breeding. Western blot analyses from total tissue homogenates demonstrated that the PARKIN protein was absent in brain and liver, thus confirming efficient disruption of *Parkin* (Fig. 1a). At 15 months of age, both male and female mice lacking PARKIN appeared healthy and showed no difference in body and heart weight when compared with age-matched controls (Fig. 1b).

We proceeded to investigate how *Parkin* ablation affects OXPHOS function in tissues with high energy demand, such as brain, heart, and skeletal muscle, of aged mice (Fig. 1c, d). No changes in steady-state levels of OXPHOS subunits were found in aged *Parkin* knockout mice in comparison with controls by using western blot analyses (Fig. 1c and Supplementary Fig. 1a). Next, we assessed OXPHOS function in brain, heart and skeletal muscle and found normal respiratory chain enzyme activities in aged mice lacking PARKIN (Fig. 1d). We measured the mtDNA copy number, as an indicator of mitochondrial mass, by using qPCR analyses with two different probes (ND1 and ND4) and found no alterations in mtDNA levels of *Parkin* knockout mice (Fig. 1e), arguing against an aberrant ongoing mitochondrial turnover in the analyzed tissues. To summarize, the age-associated deterioration of mitochondrial function is not aggravated by loss of PARKIN in key energy demanding tissues of the mouse.

Parkin loss does not exacerbate the phenotypes of mtDNA mutator mice

To investigate the debated role of PARKIN under mitochondrial stress conditions, we generated *Parkin* knockout mice that were also homozygous for the mtDNA mutator allele (*Parkin*$^{-/-}$; *PolgA*$^{mut/mut}$). The mtDNA mutator animals exhibit a premature ageing phenotype characterized by severe mitochondrial impairment caused by the progressive accumulation of mtDNA mutations[29,30]. In two previous studies, loss of PARKIN was reported to cause motor impairment and degeneration of DA neurons in mtDNA mutator mice[22,31]. At variance with these results, a third study reported neither aggravation of the ageing phenotypes nor loss of DA neurons when *Parkin* was disrupted in mtDNA mutator mice[23].

Given that maternal transmission of mtDNA mutations can be a confounding factor when mtDNA mutator mice are bred[32], we used a breeding strategy where heterozygous mtDNA mutator males were crossed to heterozygous *Parkin* knockout females (Supplementary Fig. 1b) to circumvent this problem. This breeding scheme (Supplementary Fig. 1b) generated double heterozygous mice (*Parkin*$^{+/-}$; *PolgA*$^{+/mut}$) that were intercrossed to produce four experimental groups (genotypes: *Parkin*$^{+/+}$; *PolgA*$^{+/+}$, *Parkin*$^{-/-}$; *PolgA*$^{+/+}$, *Parkin*$^{+/+}$; *PolgA*$^{mut/mut}$ and *Parkin*$^{-/-}$; *PolgA*$^{mut/mut}$) that were aged for 36 weeks. At this time point, the mtDNA mutator (*Parkin*$^{+/+}$; *PolgA*$^{mut/mut}$) animals manifested a substantial decrease in body weight (~20–25%) when compared with control (*Parkin*$^{+/+}$; *PolgA*$^{+/+}$) and *Parkin* knockout (*Parkin*$^{-/-}$; *PolgA*$^{+/+}$) mice. Notably, the weight loss that is typically observed in the mtDNA mutator mice[29] was not aggravated by *Parkin* knockout (*Parkin*$^{-/-}$; *PolgA*$^{mut/mut}$), arguing against an additive effect on the phenotype (Fig. 2a).

We proceeded to test whether *Parkin* knockout compromises OXPHOS capacity in different brain regions, i.e., hippocampus and the midbrain, of the mtDNA mutator mice. We assessed the activity of complex IV (cytochrome *c* oxidase, COX) in situ by employing histochemical double straining for COX and succinate dehydrogenase (COX/SDH) activity[33] as

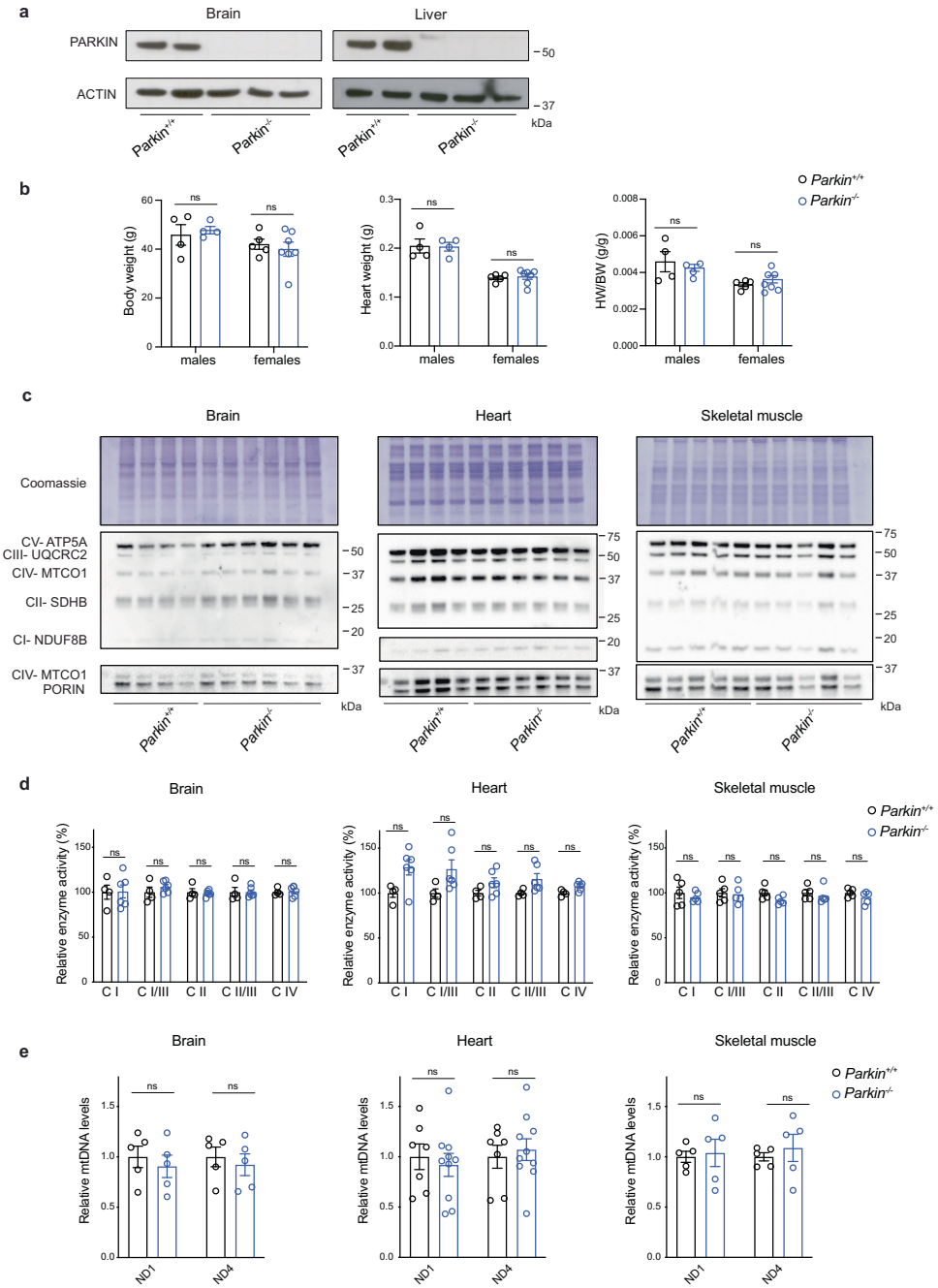

Fig. 1 | Aged *Parkin* knockout mice have normal OXPHOS function and mtDNA levels. a Western blot analysis of PARKIN protein levels in total extracts from brain and liver of control (*Parkin*$^{+/+}$) and KO (*Parkin*$^{-/-}$) mice. ACTIN was used as a loading control. **b** Body weight, heart weight and heart to body weight ratio in female and male controls and KOs at 15 months of age. Data are represented as means ± s.e.m.; $n \geq 4$ per gender; ns not significant. **c** Western blot analysis of OXPHOX subunits steady-state levels in mitochondrial protein extracts from brain, heart, and skeletal muscle. Coomassie staining and PORIN were used as loading controls. **d** Respiratory chain enzyme activity assays of CI, CI+CIII, CII, CII+CIII, and CIV in isolated mitochondria from brain, heart, and skeletal muscle (gastrocnemius and soleus). Data are represented as means ± s.e.m.; $n \geq 4$; ns not significant. **e** Quantification of mtDNA copy number performed by qPCR (ND1 and ND4/18S rRNA) in brain, heart, and skeletal muscle. Data are represented as means ± s.e.m.; $n \geq 4$; ns not significant.

well as by the nitrotetrazolium blue exclusion assay (NBTx) enzyme histochemistry[34]. As positive controls, we used the heart of mtDNA mutator mouse (Supplementary Fig. 2b) and the hippocampal sections from mitochondrial late onset neurodegeneration (MILON) mice (Fig. 2d and Supplementary Fig. 2a), which have postnatal disruption of the mitochondrial transcription factor A gene (genotype *Tfam*$^{loxP/loxP}$; +/*CamKII-cre*) causing mtDNA depletion and OXPHOS deficiency in forebrain neurons[35]. The MILON mice showed a mosaic pattern of COX deficiency with various degrees of severity (light to dark blue cells on enzyme histochemistry) in the hippocampus at 5 months of age (Fig. 2d), in line with our previous findings[35]. At 36 weeks of age, the mtDNA mutator mice (*Parkin*$^{+/+}$; *PolgA*$^{mut/mut}$) presented a clear decline in COX activity in the heart as well as in the hippocampus (Supplementary Fig. 2a, c) consistent with previous reports[33,36]. PARKIN loss did not impact on the hippocampal COX activity in mice carrying normal mtDNA (*Parkin*$^{-/-}$; *PolgA*$^{+/+}$). Furthermore, the absence of PARKIN did not worsen the mitochondrial dysfunction observed in mtDNA mutator mice (*Parkin*$^{-/-}$; *PolgA*$^{mut/mut}$) as judged by enzyme histochemistry (Supplementary Fig. 2a, c). We analyzed the midbrain and found that accumulation of mtDNA mutations (*Parkin*$^{+/+}$; *PolgA*$^{mut/mut}$) alone or in combination with PARKIN loss (*Parkin*$^{-/-}$; *PolgA*$^{mut/mut}$) did not cause any detectable decrease in COX activity *in Substantia nigra* (SN) (Fig. 2b, c, e, f). We next quantified the number of midbrain DA neurons expressing tyrosine hydroxylase (TH) in the ventral midbrain (both SN and ventral tegmental area, VTA) by using confocal microscopy (Fig. 3a, b and Supplementary Fig. 2d). No differences in DA neuron amounts were observed in the analyzed groups of animals at age of 36 weeks. These results were further supported by unaltered steady-state levels of TH protein in the ventral midbrain of these mutant mice (Fig. 3c, d). We also performed confocal analysis of brain sections to measure the number of mtDNA foci in TH positive neurons. However, we did not detect

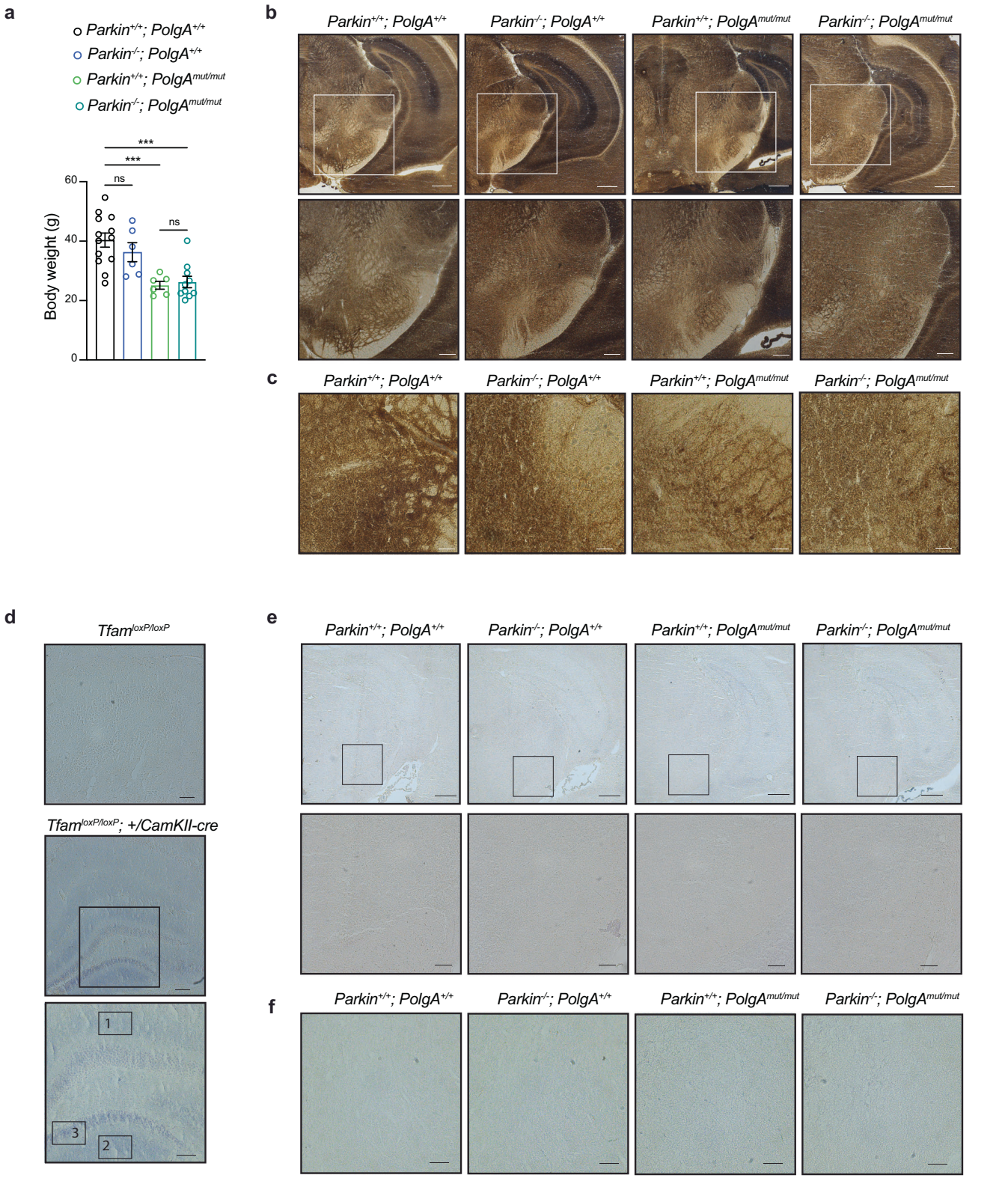

Fig. 2 | *Parkin* loss does not affect COX activity in the brain of mtDNA mutator mouse. a Body weight measured in both female and male mice at 36 weeks of age. Data are represented as means ± s.e.m.; $n \geq 6$ per group; $^{***}p < 0.001$, ns not significant. Representative images of COX enzyme activity in ventral midbrain section in 36-week-old mice measure using **b**, **c**. COX/SDH staining (Scale bars: 500 µm, 200 µm and 50 µm) and **d–f** NBTx histochemistry (Scale bars: 500 µm, 100 µm and 50 µm). Hippocampal brain sections of MILON mice (conditional *Tfam KO* in forebrain neurons, $Tfam^{loxP/loxP}$; $+/CamKII\text{-}cre^{-}$) at 5 months of age were included as positive control. Different levels of COX deficiency from mild to severe marked as 1–3, respectively.

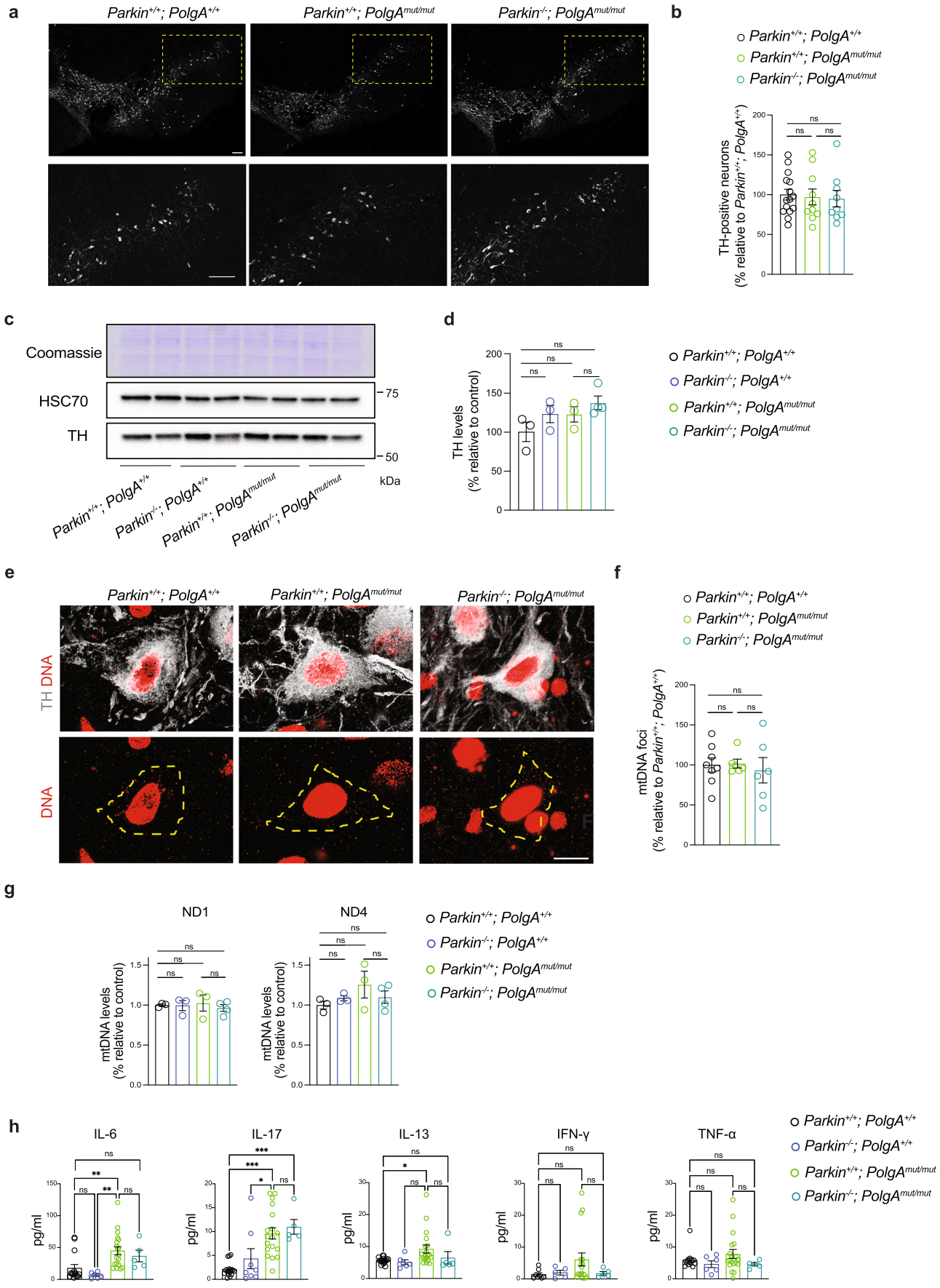
a
Parkin+/+; PolgA+/+
Parkin+/+; PolgAmut/mut
Parkin-/-; PolgAmut/mut
b
Parkin+/+; PolgA+/+
Parkin+/+; PolgAmut/mut
Parkin-/-; PolgAmut/mut
TH-positive neurons (% relative to Parkin+/+; PolgA+/+)
ns
c
Coomassie
HSC70
TH
75
50
kDa
Parkin+/+; PolgA+/+
Parkin-/-; PolgA+/+
Parkin+/+; PolgAmut/mut
Parkin-/-; PolgAmut/mut
d
TH levels (% relative to control)
e
TH DNA
DNA
f
mtDNA foci (% relative to Parkin+/+; PolgA+/+)
g
ND1
ND4
mtDNA levels (% relative to control)
h
IL-6
IL-17
IL-13
IFN-γ
TNF-α
pg/ml

Fig. 3 | *Parkin* loss does not exacerbate the phenotypes of mtDNA mutator mouse. a Representative confocal images of TH-immunostained neurons in midbrain sections (Scale bars: 100 µm). **b** Quantification of TH-positive DA neurons performed using stereological analysis. Data are represented as mean ± s.e.m.; $n \geq 5$ slices from 2-3 mice per genotype. ns not significant. **c** Western blot analysis of TH protein steady-state levels in ventral midbrain isolated from coronal brain sections. Coomassie staining and HSC70 were used as a loading control. **d** Densitometric quantification of the TH steady-state protein levels determined by western blots. Data are represented as mean ± s.e.m.; $n \geq 3$ per genotype; ns not significant. **e** Representative images of DNA staining (red) in TH+ neurons (gray) of the ventral midbrain; the area occupied by TH neurons is masked in yellow (Scale bar: 10 µm). **f** Quantification of mtDNA foci in 25–53 cells from several midbrain sections. Data are represented as mean ± s.e.m.; n≥5 slices from 2-3 mice per genotype; ns not significant. **g** Quantification of mtDNA copy number performed by qPCR (ND1 and ND4/18S rRNA) in ventral midbrain isolated from coronal brain sections. Data are represented as mean ± s.e.m.; $n \geq 3$. ns not significant. **h** Levels of inflammatory cytokines (pg/ml) in plasma samples collected from mice at 36 weeks of age. Data are represented as means ± s.e.m.; $n \geq 5$ per genotype; $^{*}p < 0.05$, $^{**}p < 0.01$, $^{***}p < 0.001$, ns not significant.

substantial changes in the number of mitochondrial nucleoids between the analyzed groups (Fig. 3e, f). In addition, no changes in mtDNA levels were found by using qPCR analysis on total homogenates of ventral midbrains (Fig. 3g). Thus, loss of PARKIN in combination with increased levels of mtDNA mutations does not impact mtDNA copy number or survival of DA neurons in the midbrain.

A recent study reported that the ablation of *Parkin* triggers inflammation induced by stimulator of interferon gene (STING) pathway in mtDNA mutator mice resulting in a profound increase in the levels of pro-inflammatory cytokines from 20 weeks of age[31]. To examine the involvement of PARKIN in mitochondria-driven innate immunity, we measured 45 circulating plasma cytokines and chemokines in the four groups of mutant mice at the age of 36 weeks (Fig. 3h and Supplementary Fig. 3a). We observed a significant increase in the levels of IL-6, IL-17 and IL-13 in mtDNA mutator mice (Fig. 3h and Supplementary Fig. 3a). There was also a clear trend, although not significant, towards increased levels in other pro-inflammatory mediators, such as IFN-γ and TNFα, in mtDNA mutator mice (Fig. 3h). Importantly, *Parkin* loss alone or in combination with the mtDNA mutator allele did not further increase levels of the 45 measured cytokines and chemokines (Fig. 3h and Supplementary Fig. 3a).

Taken together, our data show that disruption of *Parkin* does not exacerbate observed defects in the brain of the mtDNA mutator mice, which is well in line with results from a recent report[23]. In addition, we demonstrate that *Parkin* ablation does not aggravate the inflammatory phenotype caused by progressive accumulation of mtDNA mutations.

Induction of PARKIN loss in adult DA neurons does not cause neurodegeneration

Previous studies have suggested that *Parkin* knockout mice do not develop parkinsonism due to compensatory mechanisms occurring during development[13,24]. This hypothesis was further supported by the observation that deletion of *Parkin* in the adult ventral midbrain, induced by stereotaxic injections of cre-expressing adenovirus, leads to a decreased mitochondrial biogenesis and progressive degeneration of DA neurons[37,38]. To use a different and more robust approach to delete *Parkin* in midbrain DA neurons of adult mice, we generated *iParkin*^{DA} (genotype: *Parkin*$^{loxP/loxP}$, +/DatCreERT2) mice allowing the disruption of *Parkin* by tamoxifen injection (Supplementary Fig. 4a) at the age of 5–7 weeks, following a previously optimized protocol[39]. To investigate the efficiency of the inducible knockout system, we used a reporter allele expressing mitochondrially targeted YFP preceded by a loxP-flanked stop cassette (mitoYFP)[40]. As predicted, tamoxifen injection in double heterozygous (+/mitoYFP; +/Dat-cre-ERT2) mice resulted in deletion of the stop cassette and activation of YFP expression in mitochondria of TH positive (TH+) neurons (Supplementary Fig. 4b). We proceeded to disrupt *Parkin* in adult DA neurons of *iParkin*^{DA} mice by using tamoxifen injection and to test their motor performance over time. Surprisingly, when measuring horizontal and vertical (rearing) motor activities using an open-field arena system we found that *iParkin*^{DA} mice did not exhibit defects in locomotion at 20, 40 and 60 weeks after tamoxifen injection (Fig. 4a). In agreement with the absence of motor impairment, normal levels of TH positive midbrain DA neurons were detected in *iParkin*^{DA} mice at 40 and 60 weeks after tamoxifen injection (Fig. 4b, c).

In summary, our results demonstrate that genetic ablation of *Parkin* in DA neurons of the adult nigrostriatal system does not result in any detectable motor defects or neurodegeneration, which argues against the hypothesis that developmental compensatory pathways are acting in germline *Parkin* knockout mice.

Parkin-deficient neurons do not exhibit changes in the transcriptomic profile

It has been previously described that PARKIN regulates the levels of zinc finger protein 746 (ZNF746), also known as PARIS, via ubiquitination and degradation mediated by the proteasome system[38]. According to the proposed model, PARIS acts as transcriptional repressor controlling the expression of peroxisome proliferator-activated receptor gamma, coactivator 1α (PGC-1α), which, in turn, orchestrates important metabolic functions, including mitochondrial biogenesis, by sophisticated transcriptional mechanisms[37].

To investigate transcriptional responses induced by PARKIN loss in adult DA neurons we used a previously described strategy to isolate fluorophore-labeled midbrain DA neurons from adult mice[39]. We generated *iParkin*^{DA} and control mice also containing the mitoYFP allele and isolated DA neurons for bulk RNAseq analysis at 5 and 40 weeks after tamoxifen injection (Fig. 5a). For each time point, we collected mitoYFP positive and mitoYFP negative cells and prepared libraries for RNAseq analysis using Smart-seq2 protocol[41]. Extensive quality control analyses were carried out and substantial enrichment of midbrain DA neurons was verified by the expression of well-established markers for DA neurons (e.g., *Th, Ddc*, *Slc6a3*, *Nr4a2* and *En1*) in mitoYFP positive cells from controls and knockouts, whereas specific markers expressed by astrocytes and microglia (e.g., *Gfap, Slc1a3, Aldh1l1, Itgam, P2ry12 and Tmem119*) were almost undetectable (Fig. 5b, c and Supplementary Fig. 4c, d). We next performed hierarchical clustering analyses using the most variably expressed genes and found that DA neurons isolated at 5 and 40 weeks after injection could not be distinguished based on PARKIN expression (Fig. 5d). Thus, the transcriptome of *Parkin*-deficient DA neurons did not exhibit major differences in comparison with controls. Additional DESeq2 analysis (listed in Supplementary Dataset 1 and 2) of the transcriptome profiles of FACS-sorted *iParkin*^{DA} and control DA neurons showed no differentially expressed genes at an adjusted *p* value (padj) of <0.05 at 5 and 40 weeks after tamoxifen injection (Fig. 5e), consistent with the observed lack of clustering (Fig. 5d). Although no significant changes were observed in the overall expression profiles of DA neurons lacking PARKIN, we decided to further interrogate our datasets by examining levels of transcripts for specific genes previously reported to be affected by PARKIN loss. This further investigation confirmed that adult-onset ablation of *Parkin* in DA neurons did not alter the expression of *Zfn746* (PARIS), *Ppargc1a* (PGC-1α) or PGC-1α-target genes, including *Nrf1* (Fig. 5f and Supplementary Fig. 4e). In addition, the expression levels of genes encoding inflammasome (*Nlrp3)* and cGAS (*Mb21d1*)-STING (*Tmem173*) components were not affected by PARKIN loss at 5 and 40 weeks after tamoxifen injection. These results demonstrate that the genetic ablation of *Parkin* in adult DA neurons is not sufficient to trigger a substantial transcriptomic change that alone will drive or promote DA cell degeneration and death.

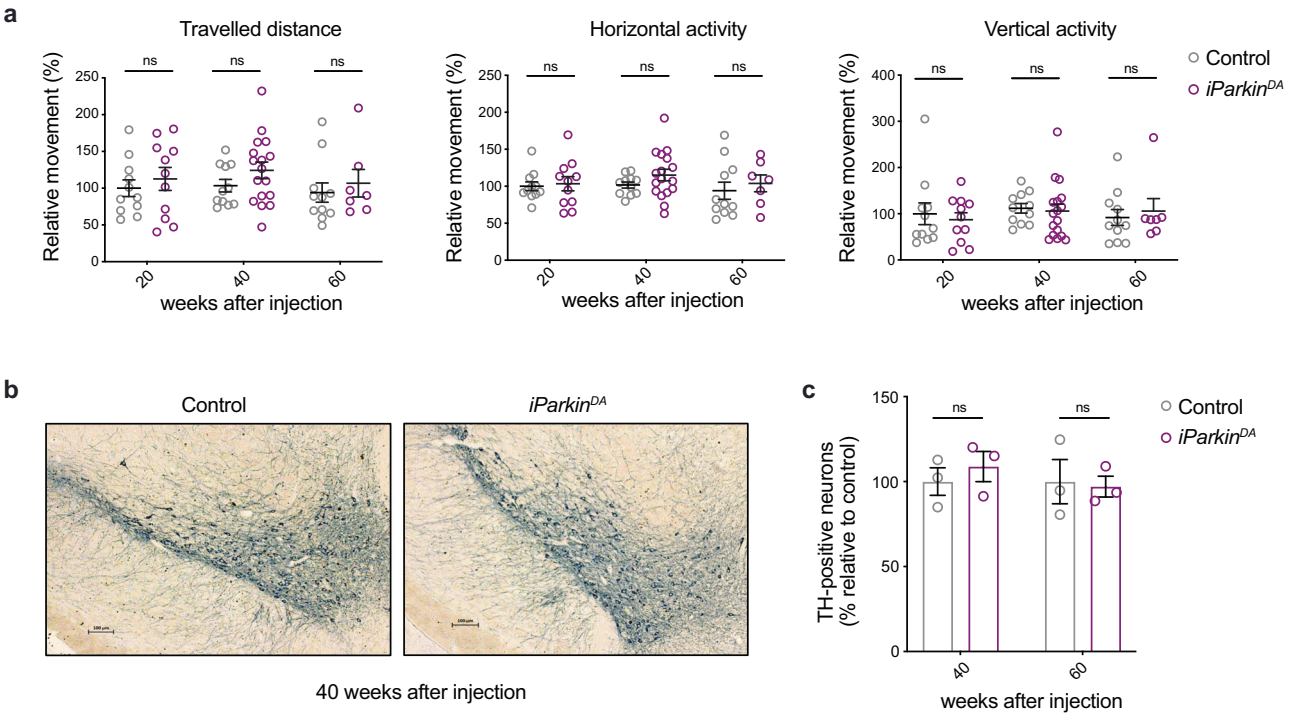

Fig. 4 | *Parkin* ablation in adult midbrain DA neurons does not lead to neurodegeneration. a Spontaneous motor activity (horizontal and vertical activity and total distance) was measured in open field arena over 60 min. Data are represented as means ± s.e.m.; $n = 7–17$; ns not significant. **b** Representative images of TH-like immunoreactivity in section from midbrain (Scale bars: 100 µm). **c** Quantification of TH-positive DA neurons in the midbrain at 40 and 60 weeks after injection. $n = 3$; ns not significant.

Normal mitochondrial function in skeletal muscle of PARKIN deficient patient

The patient of this study presented as a teenager with slowness and stiffness. At the age of 21, she was diagnosed with suspected generalized dystonia. Her symptoms slowly worsened and at age 32, she was diagnosed with PD and initiated dopaminergic medication. She has no history of hyposmia, REM sleep behavioral disorder, depression, constipation or dysautonomia. Upon examination at the time of genetic testing at the age of 51 years, she used a walker and presented with gait difficulties with freezing episodes, slightly impaired postural control, unsteadiness, discrete bilateral rigidity, and fine movements dysfunctions. She had intermittent dyskinesias but no tremor. She had no moderate or severe non-motor symptoms and received 0 points in the non-motor symptoms scale. Her cognition was intact with a MoCa score of 27 points. Her total MDS-UPDRS score was 55 points (2 + 12 + 37 + 4) and Hoehn and Yahr staging 3. A brain MRI was normal, while a [123I] ioflupane SPECT examination showed major loss of the dopamine transporter (DAT) in the basal ganglia (Fig. 6a). Automated quantification using the BRASS program showed reduced DAT uptake in nucleus caudatus and putamen bilaterally. Her symptoms were responsive to a combination of low doses of levodopa, COMT inhibitor and D2R dopamine agonist.

A detailed genetic analysis on patient biopsy performed by whole genome sequencing identified a heterozygous 11,6 kb deletion that includes the entire exon 5 of *PRKN* with an insertion of 34 nucleotides at the breakpoint; this variant is described as c.575 4062_658 + 7471delinsTAAATTAGAAAATTAATTAGAAAAATTTAAATTA, p.(Gly179_Ala206del). No other pathogenic variants were identified in the coding region or at the exon/intron boundaries. Further investigations evaluating deep intronic changes revealed the presence of two uncommon variants that were predicted to create a possible splice site: c.413-23899C>G (g. 162646183C>G) and c.535-57718A>G (g. 162532924A>G) in intron 3 and intron 4, respectively. These intronic variants were maternally inherited, while the exon 5 deletion was not present in the mother but unfortunately the DNA from the father was not available. To understand whether these variants affect *PRKN* expression, we performed RNA analysis that showed that the patient does not express a wild-type mRNA. Using primers targeting exon 1 and 7, three different RT-PCR products were amplified: one missing exon 5, as a consequence of the exon 5 deletion presumably inherited from the paternal allele, and two PCR products presented with a 102 bp sequence insertion starting from the nucleotide after the variant c.413-23899G>C. Notably, one of these two amplicons also lacked exon 4 (Fig. 6b). The same analysis performed on the maternal sample showed the presence of a wild-type product as well the two aberrant splicing products.

Although it remains unclear whether the exon skipping is due to variant c.413-23899G>C or variant c.535-57718A>G in intron 4, we proceed to investigate how the presence of the described compound heterozygous variants impacts on PARKIN protein steady-state levels. A western blot analysis of total protein extracts from fibroblasts of the patient showed absence of the PARKIN protein (Fig. 6c), confirming that the deep intronic variants indeed generate a loss-of-function allele. To study the effect of PARKIN loss in adult human tissues and mitochondria, a muscle biopsy was obtained from the anterior tibial muscle of the patient using a conchotome and mitochondria were isolated. Assessment of the OXPHOS function showed normal respiratory chain enzyme activities (Fig. 6d) and normal ATP production rates (Fig. 6e) in skeletal muscle. In addition, histopathological examinations performed in the PD patient and in an age- and gender-matched healthy individual revealed that skeletal muscle tissue was well preserved without any necrotic fibers or inflammatory cell infiltrates (Fig. 6f). COX/SDH staining identified the presence of a single COX-deficient fiber in both the patient and control individual (Fig. 6f and Supplementary Fig. 5a), compatible with the age of the subjects and in line with normal NADH and SDH staining (Supplementary Fig. 5b). Staining for glycogen and neutral lipid were also normal (Supplementary Fig. 5b) and no ragged-red muscle fibers were detected using Gomori trichrome staining (Fig. 6f). In addition, transmission electron microscopy showed no alterations in muscle morphology and mitochondrial ultrastructure (Fig. 6g and Supplementary Fig. 5a).

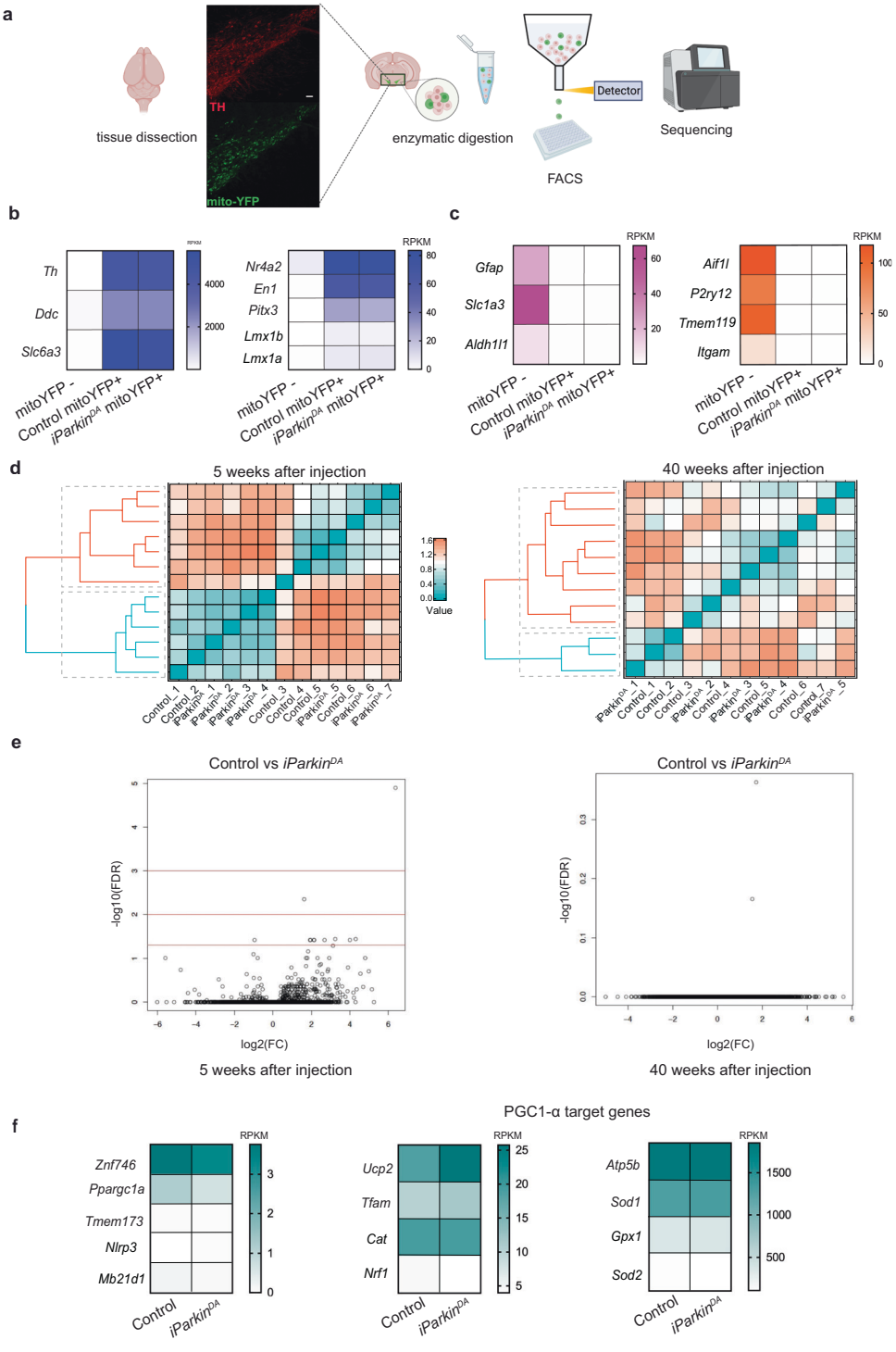

Fig. 5 | *Parkin*-deficient midbrain DA neurons do not exhibit changes in the transcriptomic profile. a Experimental workflow of RNAseq in FACS-sorted DA neurons. The isolation was performed using mice expressing the mito-YFP allele under the control of the DA transporter (DAT, *Slc6a3*) promoter. Fluorescently labeled mitochondria (green) were visible in TH-expressing neurons (red) of the midbrain. Vibratome sections from mouse brains were enzymatically digested and mechanically triturated resulting in a single cell suspension; fluorescently labeled midbrain DA neurons were collected by FACS; mitoYFP positive and negative cells were used for bulk-RNAseq. Heatmaps showing the expression levels of genes encoding **b** DA neuronal markers, **c** astrocyte and microglial markers in mitoYFP+ and mitoYFP− samples (Reads Per Kilobase Million, RPKM) at 40 weeks after injection. **d** Hierarchical clustering analysis of RNAseq data from DA neurons isolated from *iParkin*^{DA} and control mice at 5 weeks (left panel) and 40 weeks (right panel) after tamoxifen injections. $n > 5$ per genotype and time point. **e** Volcano plot displaying differential gene expression at 5 and 40 weeks after injections. **f** Heatmap showing the expression of genes involved in mitochondrial biogenesis and inflammation in mitoYFP+ cells isolated from *iParkin*^{DA} and control mice at 40 weeks after injection.

Discussion

Although our results argue against a critical function for PARKIN in maintaining OXPHOS capacity, it should be emphasized that PARKIN is highly conserved across species[42] and is present in both vertebrates, e.g., human, rat, mouse, bird, frog, and invertebrates, e.g., fruit-flies. The gene encoding PARKIN has thus been maintained by selection during evolution of metazoa and must therefore have an important function. Biochemically, PARKIN is a ubiquitin E3 ligase that mediates the covalent binding of mono ubiquitin or ubiquitin chains to lysine residues of proteins. The conjugation of a single ubiquitin moiety regulates the activity, the interactions, or the trafficking of PARKIN substrates, whereas polyubiquitination marks them for degradation by the proteasome or lysosome[43]. PARKIN consists of an N-terminal ubiquitin-like (Ubl) domain and four zinc-finger domains, RING0, RING1, IBR and RING2. Several crystal structures of PARKIN and its different domains have been solved with various degrees of resolution[44–47], which have clarified important molecular aspects of PARKIN activation and regulation. In addition, these structural studies have significantly contributed to unveil how loss-of-function mutations can disrupt protein function by compromising the zinc coordination, the protein folding, the catalytic site, or the protein contact sites[48]. Affinity purification techniques coupled with quantitative mass spectrometry analyses have shown that PARKIN can interact and promote the ubiquitination of a

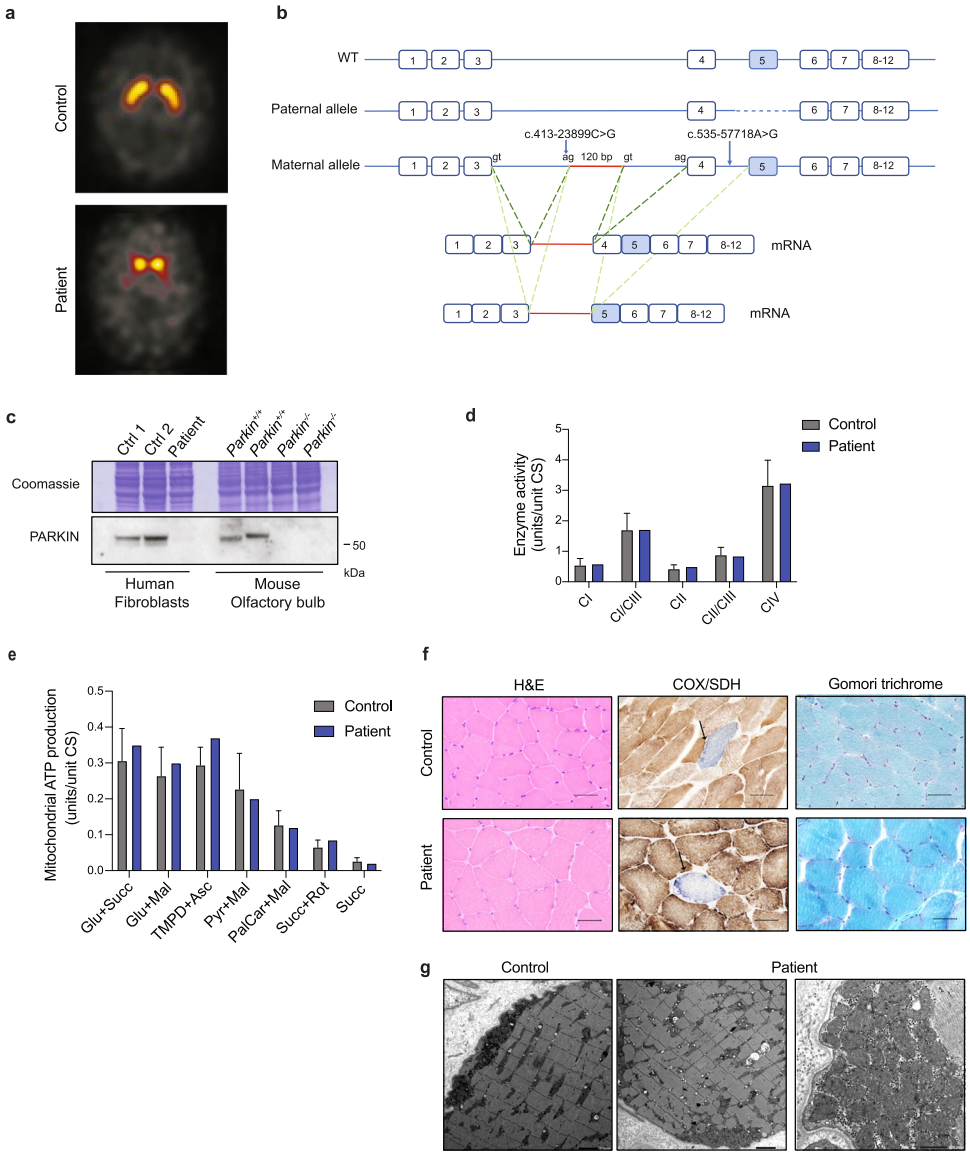

Fig. 6 | Loss of PARKIN in a PD-patient does not affect the OXPHOS function in skeletal muscle. a DaTSCAN® SPECT of presynaptic dopaminergic terminals in the striatum in a control subject and the PARKIN deficient PD patient. **b** The wild type *PRKN* gene and alleles identified in the patient. Results of the mRNA analysis of the maternal allele are shown. In red the 120 bp intronic sequence inserted in the mRNA. Additional AG and GT splicing sites are indicated. **c** Western blot analysis of PARKIN steady-state levels in total protein extracts from control subjects and the *PRKN* PD patient. The antibody used for PARKIN detection is raised against an amino acid sequence partially encoded by exons 4 and 5 of *PRKN* gene, which are affected in *PRKN* patient. Total extracts from olfactory bulb of control ($Parkin^{+/+}$) and KO ($Parkin^{-/-}$) mice were used as reference. **d** Enzyme activity assays of CI, CI+CIII, CII, CII +CIII, and CIV in isolated mitochondria from skeletal muscle from controls and the patient. **e** The mitochondrial ATP production rate in isolated mitochondria from skeletal muscle from controls and the patient. **f** Skeletal muscle histopathology using staining for hematoxylin and eosin (H&E), COX/SDH and Gomori trichrome in the *PRKN* patient and an age- and gender-matched healthy subject (Scale bar: 50 µm). **g** Transmission electron microscopy analysis showing muscle morphology and mitochondrial ultrastructure in *PRKN* patient and age- and gender-matched control (Scale bar: 2 µm and 500 nm).

multitude of substrates without targeting a specific consensus sequence or a structural recognition motif, suggesting that PARKIN has a relatively lax specificity and the proximity to the substrate is important for the ubiquitination[49]. Despite the lack of consensus sequence, it is possible that PARKIN substrates have a common modification or state, but to date the mechanisms for substrate recognition remain largely unknown.

The broad range of PARKIN substrates has linked its function with the regulation of mitochondrial integrity. In fact, PARKIN can ubiquitinate both mitofusin 1 and 2 (MFN1 and MFN2), which are the main the players in mitochondrial fusion, and target them for proteasomal degradation[49–52]. In addition, PARKIN has been implicated in the regulation of mitochondrial biogenesis, primarily through the ubiquitination and subsequent proteasomal degradation of PARIS, which is a PGC1-α repressor[37,38]. Furthermore, PARKIN, together with the serine-threonine kinase PINK1, has been reported to function as a crucial regulator of mitochondrial degradation via mitophagy. According to this model, PARKIN is activated by PINK1 in response to mitochondrial damage and thereafter ubiquitinates a variety of OMM proteins. This process is supposed to mark functionally impaired mitochondria for engulfment by the autophagosome followed by degradation in the lysosome[53]. However, in vivo studies in fruit flies and mice have questioned the contribution of PINK1/PARKIN-mediated mitophagy under basal conditions[16,54] or in response to mitochondrial damage[40]. Interestingly, a recent study conducted using human iPSC-derived DA neurons proposes a new function of PARKIN in promoting mitochondrial and lysosomal amino acid homeostasis through stabilization of inter-organelle contacts[55].

In this work, we addressed fundamental questions about the role of PARKIN in mitochondria during ageing or upon mitochondrial stress in vivo. We demonstrate here that loss of *Parkin* in the mouse does not aggravate the naturally occurring decline in mitochondrial function of high-energy-demanding tissues. Our findings argue that PARKIN is not required to sustain tissue bioenergetics during ageing. In addition, *Parkin*-deficient mice present normal mtDNA levels, suggesting that PARKIN loss does not cause drastic changes in mitochondrial mass. Hence, these results do not support a major involvement of PARKIN in mitochondrial quality control, which suggests the existence of PINK1/PARKIN-independent pathways acting in the regulation of the fine balance between mitochondrial degradation and biogenesis. Recent reports have shown that loss of FBXL4, which is a subunit of the Skp1-cullin1-F-box (SCF) E3 ubiquitin ligase protein complex, increases mitophagy[56]. Loss of FBXL4 decreases the mitochondrial mass with concomitant mtDNA depletion and mitochondrial dysfunction in affected tissues in humans[57–59] and mice[56]. Three independent recent reports have shown that FBXL4 actively suppresses mitophagy by degrading the mitophagy receptors NIX and BNIP3[60–62]. The absence of FBXL4 thus

increases the levels of these receptors leading to increased mitophagy, which, in turn, causes mtDNA depletion and impaired OXPHOS function in affected patients. In contrast to PARKIN, FBXL4 and its downstream targets thus provide an important example of a clinically relevant mitophagy pathway whose impairment causes severe mitochondrial disease.

It has been reported that stress induced by mtDNA mutations results in activation of the STING-mediated innate immune response when PARKIN is absent, leading to degeneration of DA neurons and motor impairment in mice[22,31]. Using a variety of molecular and biochemical analyses, we show here that PARKIN loss does not exacerbate the proinflammatory response or neurodegeneration of mtDNA mutator mice consistent with the results from a recent independent study[23]. Importantly, also in *Drosophila* the role of STING in the induction of *Parkin* mutant phenotypes remains controversial. In fact, two recent investigations have generated conflicting results on the impact of STING loss in suppressing behavioral and mitochondrial defects manifested by *Parkin* deficient fruit flies[63,64].

Homozygous *Parkin* knockout mice do not develop parkinsonism and this failure to reproduce the human phenotype has been attributed to compensatory mechanisms activated during development. In line with this proposal, it has been reported that PARKIN loss induced by stereotaxic injection of adenovirus expressing cre-recombinase in adult mice homozygous for a lox P-flanked *Parkin* allele results in mitochondrial dysfunction and DA neuron death triggered by the transcriptional repression of PGC-1α[37,38]. We generated mice lacking PARKIN in adult midbrain DA neurons by using a tamoxifen-inducible cre-recombinase expressed under control of the DA transporter (DAT, *Slc6a3*) promoter. Surprisingly, these inducible knockout mice preserve their motor abilities and have normal levels of TH+ neurons in the midbrain. Moreover, RNA-seq analyses of isolated *Parkin*-deficient DA neurons did not reveal substantial transcriptional changes, including the transcript levels of PGC-1α-target genes. It is unclear why our results are at variance with the previous reports showing a clear phenotype after adult-onset knockout of *Parkin*. A likely explanation of the discrepancy between our results and the previous reports may lie in the different modes of expressing cre-recombinase (virus vs transgene). In fact, while the transgenic approach is genetically specific, viral approaches may cause recombination in other cell types besides DA neurons or have toxic effects when injected at higher titer doses.

In summary, we here provide compelling evidence that PARKIN is dispensable for the maintenance of OXPHOS function in adult mouse tissues, including DA neurons. These findings have been further validated in a PARKIN-deficient patient. By using whole genome sequencing, we found that the analyzed patient carries a large deletion encompassing exon 5 and two deep intronic variants, which leads to PARKIN loss. While other exon 5 deletions were previously described in PD patients[65,66], to our knowledge the pathogenicity of deep intronic variants in the *PRKN* gene was never demonstrated before. The only described splicing variants (see HGMD® Professional 2023.2) are either located at the canonical splice site or within 20 nucleotides from the intron/exon junction. Therefore, this case highlights the importance of the use of whole genome sequencing and rare intronic variants analysis to improve the diagnosis of *PRKN*-PD patients. Importantly, the patient of this study presents normal tissue morphology and preserved respiratory chain function in skeletal muscle three decades after onset of PD symptoms, which support that PARKIN is not required to maintain OXPHOS function in adult human skeletal muscle and corroborate our findings in the mouse.

Methods

Ethics statement

All animal procedures were conducted in accordance with European, national, and institutional guidelines and protocols were approved by the Stockholms djurförsöksetiska nämnd, Sweden and by the Landesamt für Natur, Umwelt und Verbraucherschutz Nordrhein–Westfalen, Germany. Animal work was performed in accordance with the recommendation and the guidelines of the Federation of European Laboratory Animal Science Associations (FELASA).

The clinical part of the study was approved by the regional ethics committee in Stockholm and the Swedish ethical review authority (2019-04967). Informed consent was obtained from *PRKN* patient and healthy subject.

Mouse models

Homozygous mice for a *LoxP*-flanked *Parkin* allele (*Parkin*$^{loxP/loxP}$) were crossed to heterozygous β-actin-cre or DATcreERT2 mice in order to generated germline whole-body knockout (*Parkin*$^{-/-}$) and adult conditional knockout (*iParkin*^{DA}) mice, respectively. At 5–7 weeks of age, *iParkin*^{DA} and control mice were treated for 5 consecutive days by intraperitoneal injection of 2 mg of tamoxifen (Sigma T5648 dissolved in ethanol and sunflower oil) to induce the ablation of *Parkin* gene in adult DA neurons. *PolgA* mutator allele (*PolgA*$^{mut/mut}$), expressing the exonuclease-deficient PolgA[29], and the stop–mito–YFP allele[40], expressing a mitochondrially targeted YFP, were subsequently introduced via additional crossing. Analyses of control and KO mice were performed at different time points. All mice were on the C57BL/6N genetic background.

Western Blot

Isolation of mitochondria from mouse heart, skeletal muscle and brain was performed by differential centrifugation[67]. Total extracts were prepared from mouse ventral midbrain isolated from coronal brain cryosections and from control and patient fibroblasts using RIPA buffer supplemented with protease inhibitors (Complete, Roche). Five micrograms of isolated mitochondria or twenty micrograms of total protein extracts were resuspended in Laemmli buffer, run on 12% SDS–polyacrylamide gel electrophoresis (Invitrogen) and then transferred onto nitrocellulose membrane using *iBlot2* system (Invitrogen). Immunodetection was performed according to standard techniques using enhanced chemiluminescence Immun-Star HRP Luminol/Enhancer (Bio-Rad). The following antibodies were used: PORIN (ab14734, Abcam), PARKIN (ab15494, Abcam), TH (MAB318, Chemicon), HSC70 (sc-7298, Santa Cruz) and OXPHOS Rodent Antibody Cocktail (ab110413, Abcam) for NDUFB8 (CI), SDHB (CII), UQCRC2 (CIII), MTCO1 (CIV) ATP5A (CV).

All blots were processed in parallel and derive from the same experiments. Quantification of Western blot signals was performed by densitometry using software FIJI (ImageJ2; Version 2.3.0/1.53f).

Biochemical evaluation of respiratory chain function and ATP production

Respiratory chain enzyme activities and ATP production were measured in isolated mitochondria from different mouse and human tissues, as previously described[68].

mtDNA copy number

Genomic DNA was isolated from snap-frozen tissues or from ventral midbrain isolated from coronal brain cryosections using the DNeasy Blood and Tissue Kit (Qiagen), according to the manufacturer's instructions. Quantification of mtDNA copy number was performed in triplicates using five ng of DNA using TaqMan Universal Master Mix II and TaqMan probes from Life Technologies. The mtDNA levels were assessed using probes against the mitochondrial genes (ND1 and ND4), and nuclear 18*S* rRNA gene was used as a loading control.

Motor performance

Motor activity of control and *iParkin*^{DA} mice was measured in open field arenas (VersaMax, AccuScan Instruments) at 20, 40, and 60 weeks after tamoxifen injection. Following an acclimation period of at least 30 min in the ventilated experimental room, mice were placed individually in activity cages (40 × 40 cm and 30 cm high) for 60 min. A grid of infrared light beams was used to record spontaneous horizontal and vertical activities and the total distance traveled was calculated.

Cytokines and chemokines quantification

After cervical dislocation, blood was collected by cardiac puncture in anticoagulant-treated tubes (EDTA tubes BD) and plasma (supernatant) was obtained after centrifugation at 2000 × *g* for 10 min at 4 °C. Plasma aliquots were snap-frozen in liquid nitrogen and stored at −80 °C until the analysis. Mouse Cytokines/Chemokines were quantified using the 45-Plex Discovery Assay® Array (MD45) by Eve Technologies.

Immunohistochemistry and confocal microscopy

Anesthetized mice were perfused with 4% paraformaldehyde in phosphate buffer. The brains were dissected, postfixed for 2 h, and equilibrated with 10% sucrose. Brains were frozen and cryo-sectioned to obtain 14–20-µm thick sections. After 1 h in blocking solution (PBS + 0.3% Triton X-100 + 1% BSA), the tissue sections were immunolabeled overnight with primary antibodies against TH (1:1000, Chemicon). For fluorescent staining, Cy3- (1:400, Jackson Biolabs), Alexa 546- (1:400, Life Technologies) and Alexa 633- conjugated secondary antibodies (1:400, Life Technologies) were used. Confocal images were acquired by sequential scanning using a LSM800 or LSM880 microscope (Zeiss).

Alternatively, fixed brains were transferred in PBS and sectioned into 50-um thick coronal slices on a Leica vibratome (Leica Microsystems GmbH, Vienna, Austria). Free-floating slices were placed in tris-EDTA buffer (pH 9) for 30 min at 80 °C for antigen retrieval and were then blocked for 15 min with 3% BSA in PBS at room temperature (RT). Slices were subsequently incubated overnight at 4 °C under agitation with the primary antibodies: anti-tyrosine hydroxylase (1:500, Synaptic System) and anti-DNA (1:200, Progen). Sections were then incubated with secondary antibodies conjugated with Alexa 488 and Alexa 594 at a dilution of 1:500 for 2 h at RT. Afterwards, slices were thoroughly washed in PBS, counterstained with DAPI, and mounted on microscopic slides with AquaPolymount. Slices were imaged with a laser scanning confocal Stellaris 5 or TCS SP8 gSTED equipped with a white light laser and a 405-diode ultraviolet laser (Leica Microscope). Image acquisition was done using the LAS-X software in accordance with the Nyquist sampling sequential mode by exciting the fluorophores and collecting their signal with hybrid detectors (HyDs).

Image processing

Acquired images were deconvolved using the Hyugens Professional (Huygens Pro, Scientific Volume Imaging) to improve contrast and resolution. For further image processing Image J and Adobe Photoshop were used to adjust brightness and contrast. For figure preparation Adobe Illustrator was used.

Quantification of TH+ neurons

Every sixth midbrain cryo-section (20 µm thickness) was immunolabeled for TH. For the non-fluorescent labeling, a biotinylated secondary antibody (1:400, Vector Laboratories) was used and the signal was detected by using a peroxidase substrate (Vector SG, Vector Laboratories). Nuclei of TH-positive neurons were counted in both right and left hemisphere from 9–11 sections for brain. For experiments involving vibratome sections, briefly, 4–5 midbrain sections per mouse were selected based on anatomical reference atlases (e. g., Allen Brain Atlas) to minimize brain region variability in sampling among experimental groups. The number of TH positive neurons was assessed in both hemisphere using a stereology-based method as well as Cell Counter plugin (Image J software). Stereological quantification was carried out using the optical dissector method facilitated by an ImageJ macro adapted from Aleksandr Mironov, University of Manchester (github.com/ImageJ_stereology). The macro inserted an unbiased brick pattern, which covered 10% of the stack volume in 36 bricks. The quantification was accomplished by counting the number of bricks, which fell into the reference space, i.e. the midbrain and the number of TH positive neurons inside an unbiased brick without touching any forbidden surface. Density of the TH+ neurons was calculated according to this formula: $\widehat{N\nu} = \frac{1}{a/g \cdot h} \cdot \frac{\Sigma Q-}{\Sigma P}$ ($\widehat{N}$ = estimate of numerical density, a/f = Area of frame, h = dissector height, $\Sigma Q-$ Sum of particles counted, ΣP = Sum of frame associated points hitting reference space). When using Cell Counter plugin, the quantification was performed by dividing the number of counted TH + cells by the area occupied by the counted cells. To avoid bias, operator was kept blind to the genotype of the samples throughout the analyses.

Dual COX/SDH enzyme histochemistry

Brains from the four experimental groups were rapidly collected and frozen on dry ice. Brain sections (20 µm) were stained as previously described[69].

NBTx enzyme histochemistry

NBTx enzyme histochemistry was performed as previously reported[34]. Briefly, 20 µm brain sections were equilibrated 5 min in PBS. Slides were then incubated at room temperature in freshly prepared NBTx staining solution (15 mM Nitrotetrazolium Blue Chloride, 0.2 mM Phenazine Methosulfate, 130 mM Sodium Succinate in PBS pH 7). After 90 min, samples were washed three times in PBS, dehydrated in increasing concentration EtOH solutions (50%, 70%, 96%, 100%) and in xylene and finally mounted in Cytoseal.

Isolation of DA neurons by FACS

Brains were dissected from mitoYFP expressing mice, sectioned and dissociated into single cell suspensions, as previously described[70]. After dissociation, mitoYFP positive and negative cells were collected using a BD FACSAria III Cell Sorter for RNAseq analysis.

Library preparation and sequencing

FACS sorted cells ($n > 5$ per genotype) were used to generate the cDNA libraries according to the Smartseq2 protocol as previously described[41]. The Nextera XT DNA library preparation kit (FC-131-1024) was used for cDNA tagmentation. The quality of cDNA and tagmented cDNA was checked on a High-Sensitivity DNA chip (Agilent Bioanalyzer). Sequencing was performed on Illumina HiSeq 2500, giving 51 bp reads after de-multiplexing.

Reads were aligned to the mouse genome (mm10) merged with eGFP and ERCC spike-in sequences using Star v2.3.0 and filtered for uniquely mapping reads. Gene expression was calculated as read counts and as reads per kilobase gene model and million mappable reads (RPKMs) for each transcript in Ensembl release 75 using rpkmforgenes. Read counts were summed across technical replicates resulting in gene expression data. Protein-coding genes were selected for further analyses.

Hierarchical clustering was performed in R using the ward.D2 agglomerative method and the Pearson correlation-based distance measure. Differential gene expression analysis was performed using DESeq2[71].

DaTSCAN SPECT

Assessment of presynaptic dopamine transporter with ^{123}I-labeled N-(3-fluoropropyl)-2β-carbomethoxy-3β-(4-iodophenyl)nortropane (FP-CIT) (i.e. DaTSCAN®) was done at the level of striatum according to standard clinical procedure[72].

Genetic investigation

Whole genome analysis was performed on a Illumina platform described[73]. Splicing predictions were performed by the software Alamut Visual Plus version 1.7 © SOPHiA GENETICS. RNA was extracted by whole blood collected on PAXgene™ Blood RNA tubes (Becton Dickinson) by the PAXgene™ Blood RNA Kit (Qiagen). The High Capacity cDNA Reverse Transcription Kit (Applied Biosystem) was used to synthetize cDNA; primers for RT-PCR were designed within exon1 (PRKN-1F: 5′-CACCTACCCAGTGACCATGA-3′) and exon7 (PRKN-7R: 5′-CTGCCGATCATTGAGTCTTG). Sanger sequencing was performed using the Big Dye Terminator v3.1 Cycle Sequencing Kit (Applied Biosystems) and the DNA analyzer 3500XL (Applied Biosystems). The reference sequence NM_004562.3 was used for *PRKN* gene.

Histopathological tissue analysis

Skeletal muscle biopsy from the anterior tibial muscle was snap-frozen in isopentane cooled by dry ice for cryostat sectioning. Standard techniques

were applied for histological stains and enzyme histochemistry including the oxidative enzymes NADH, SDH, COX and COX-SDH[74]. A small specimen was fixed in buffered glutaraldehyde and embedded in epoxy resins for electron microscopy according to standard procedures.

Statistical analysis

All statistical analyses were performed using GraphPad Prism v9 software. All data are in the figures are presented as mean ± s.e.m. Statistical comparisons were performed using single or multiple Student's *t* test or one-way analysis of variance (ANOVA).

Data availability

The RNA-seq dataset generated and analyzed during the current study is available in NCBI's Gene Expression Omnibus with accession number GSE263057. Additional data generated or analyzed in this study are included in the published article and the supplementary information.

Code availability

The code used for differential gene expression analysis was generated using standard DESeq2's variance model.

Received: 12 September 2023; Accepted: 11 April 2024;
Published online: 29 April 2024

References

1. Matsumine, H. et al. Localization of a gene for an autosomal recessive form of juvenile Parkinsonism to chromosome 6q25.2-27. *Am. J. Hum. Genet.* **60**, 588–596 (1997).
2. Kitada, T. et al. Mutations in the parkin gene cause autosomal recessive juvenile parkinsonism. *Nature* **392**, 605–608 (1998).
3. Lücking, C. B. et al. Association between Early-Onset Parkinson's Disease and Mutations in the *Parkin* Gene. *N. Engl. J. Med.* **342**, 1560–1567 (2000).
4. Kilarski, L. L. et al. Systematic Review and UK-Based Study of *PARK2 (parkin), PINK1, PARK7 (DJ-1)* and *LRRK2* in early-onset Parkinson's disease. *Mov. Disord.* **27**, 1522–1529 (2012).
5. West, A. B. & Maidment, N. T. Genetics of parkin-linked disease. *Hum. Genet.* **114**, 327–336 (2004).
6. Kasten, M. et al. Genotype-Phenotype Relations for the Parkinson's Disease Genes *Parkin*, *PINK1*, *DJ1:* MDSGene Systematic Review. *Mov. Disord.* **33**, 730–741 (2018).
7. Lubbe, S. J. et al. Assessing the relationship between monoallelic PRKN mutations and Parkinson's risk. *Hum. Mol. Genet.* **30**, 78–86 (2021).
8. Shimura, H. et al. Familial Parkinson disease gene product, parkin, is a ubiquitin-protein ligase. *Nat. Genet.* **25**, 302–305 (2000).
9. Ge, P., Dawson, V. L. & Dawson, T. M. PINK1 and Parkin mitochondrial quality control: a source of regional vulnerability in Parkinson's disease. *Mol. Neurodegener.* **15**, 20 (2020).
10. Narendra, D., Tanaka, A., Suen, D.-F. & Youle, R. J. Parkin is recruited selectively to impaired mitochondria and promotes their autophagy. *J. Cell Biol.* **183**, 795–803 (2008).
11. Matsuda, N. et al. PINK1 stabilized by mitochondrial depolarization recruits Parkin to damaged mitochondria and activates latent Parkin for mitophagy. *J. Cell Biol.* **189**, 211–221 (2010).
12. Kauppila, T. E. S., Kauppila, J. H. K. & Larsson, N.-G. Mammalian Mitochondria and Aging: An Update. *Cell Metab.* **25**, 57–71 (2017).
13. Whitworth, A. J. & Pallanck, L. J. PINK1/Parkin mitophagy and neurodegeneration—what do we really know in vivo. *Curr. Opin. Genet Dev.* **44**, 47–53 (2017).
14. Park, J. et al. Mitochondrial dysfunction in Drosophila PINK1 mutants is complemented by parkin. *Nature* **441**, 1157–1161 (2006).
15. Greene, J. C. et al. Mitochondrial pathology and apoptotic muscle degeneration in *Drosophila parkin* mutants. *Proc. Natl Acad. Sci.* **100**, 4078–4083 (2003).
16. Lee, J. J. et al. Basal mitophagy is widespread in Drosophila but minimally affected by loss of Pink1 or parkin. *J. Cell Biol.* **217**, 1613–1622 (2018).
17. Cornelissen, T. et al. Deficiency of parkin and PINK1 impairs age-dependent mitophagy in Drosophila. *Elife* **7**, e35878 (2018).
18. Goldberg, M. S. et al. Parkin-deficient Mice Exhibit Nigrostriatal Deficits but Not Loss of Dopaminergic Neurons. *J. Biol. Chem.* **278**, 43628–43635 (2003).
19. von Coelln, R. et al. Loss of locus coeruleus neurons and reduced startle in parkin null mice. *Proc. Natl Acad. Sci.* **101**, 10744–10749 (2004).
20. Noda, S. et al. Loss of Parkin contributes to mitochondrial turnover and dopaminergic neuronal loss in aged mice. *Neurobiol. Dis.* **136**, 104717 (2020).
21. Peker, N., Donipadi, V., Sharma, M., McFarlane, C. & Kambadur, R. Loss of *Parkin* impairs mitochondrial function and leads to muscle atrophy. *Am. J. Physiol. Cell Physiol.* **315**, C164–C185 (2018).
22. Pickrell, A. M. et al. Endogenous Parkin Preserves Dopaminergic Substantia Nigral Neurons following Mitochondrial DNA Mutagenic Stress. *Neuron* **87**, 371–381 (2015).
23. Scott, L. et al. The Absence of Parkin Does Not Promote Dopamine or Mitochondrial Dysfunction in PolgA $^{D257A/D257A}$ Mitochondrial Mutator Mice. *J. Neurosci.* **42**, 9263–9277 (2022).
24. Pinto, M., Nissanka, N. & Moraes, C. T. Lack of Parkin Anticipates the Phenotype and Affects Mitochondrial Morphology and mtDNA Levels in a Mouse Model of Parkinson's Disease. *J. Neurosci.* **38**, 1042–1053 (2018).
25. Sato, S. et al. Decline of striatal dopamine release in parkin-deficient mice shown by ex vivo autoradiography. *J. Neurosci. Res.* **84**, 1350–1357 (2006).
26. Perez, F. A. & Palmiter, R. D. Parkin-deficient mice are not a robust model of parkinsonism. *Proc. Natl Acad. Sci.* **102**, 2174–2179 (2005).
27. Larsson, N.-G. Somatic Mitochondrial DNA Mutations in Mammalian Aging. *Annu. Rev. Biochem.* **79**, 683–706 (2010).
28. Bratic, A. & Larsson, N.-G. The role of mitochondria in aging. *J. Clin. Investig.* **123**, 951–957 (2013).
29. Trifunovic, A. et al. Premature ageing in mice expressing defective mitochondrial DNA polymerase. *Nature* **429**, 417–423 (2004).
30. Kujoth, G. C. et al. Mitochondrial DNA Mutations, Oxidative Stress, and Apoptosis in Mammalian Aging. *Science* **309**, 481–484 (2005).
31. Sliter, D. A. et al. Parkin and PINK1 mitigate STING-induced inflammation. *Nature* **561**, 258–262 (2018).
32. Ross, J. M. et al. Germline mitochondrial DNA mutations aggravate ageing and can impair brain development. *Nature* **501**, 412–415 (2013).
33. Ross, J. M. Visualization of Mitochondrial Respiratory Function using Cytochrome C Oxidase/Succinate Dehydrogenase (COX/SDH) Double-labeling Histochemistry. *J.Vis. Exper.* https://doi.org/10.3791/3266 (2011).
34. Simard, M.-L., Mourier, A., Greaves, L. C., Taylor, R. W. & Stewart, J. B. A novel histochemistry assay to assess and quantify focal cytochrome *c* oxidase deficiency. *J. Pathol.* **245**, 311–323 (2018).
35. Sörensen, L. et al. Late-Onset Corticohippocampal Neurodepletion Attributable to Catastrophic Failure of Oxidative Phosphorylation in MILON Mice. *J. Neurosci.* **21**, 8082–8090 (2001).
36. Ross, J. M. et al. High brain lactate is a hallmark of aging and caused by a shift in the lactate dehydrogenase A/B ratio. *Proc. Natl Acad. Sci.* **107**, 20087–20092 (2010).
37. Stevens, D. A. et al. Parkin loss leads to PARIS-dependent declines in mitochondrial mass and respiration. *Proc. Natl Acad. Sci.* **112**, 11696–11701 (2015).
38. Shin, J.-H. et al. PARIS (ZNF746) Repression of PGC-1α Contributes to Neurodegeneration in Parkinson's Disease. *Cell* **144**, 689–702 (2011).

39. Filograna, R. et al. Mitochondrial dysfunction in adult midbrain dopamine neurons triggers an early immune response. *PLoS Genet.* **17**, e1009822 (2021).
40. Sterky, F. H., Lee, S., Wibom, R., Olson, L. & Larsson, N.-G. Impaired mitochondrial transport and Parkin-independent degeneration of respiratory chain-deficient dopamine neurons in vivo. *Proc. Natl Acad. Sci. USA* **108**, 12937–12942 (2011).
41. Picelli, S. et al. Smart-seq2 for sensitive full-length transcriptome profiling in single cells. *Nat. Methods* **10**, 1096–1098 (2013).
42. Horowitz, J. M. et al. Immunodetection of Parkin protein in vertebrate and invertebrate brains: a comparative study using specific antibodies. *J. Chem. Neuroanat.* **21**, 75–93 (2001).
43. Joch, M. et al. Parkin-mediated Monoubiquitination of the PDZ Protein PICK1 Regulates the Activity of Acid-sensing Ion Channels. *Mol. Biol. Cell* **18**, 3105–3118 (2007).
44. Riley, B. E. et al. Structure and function of Parkin E3 ubiquitin ligase reveals aspects of RING and HECT ligases. *Nat. Commun.* **4**, 1982 (2013).
45. Trempe, J.-F. et al. Structure of Parkin Reveals Mechanisms for Ubiquitin Ligase Activation. *Science* **340**, 1451–1455 (2013).
46. Wauer, T. & Komander, D. Structure of the human Parkin ligase domain in an autoinhibited state. *EMBO J.* **32**, 2099–2112 (2013).
47. Kumar, A. et al. Disruption of the autoinhibited state primes the E3 ligase parkin for activation and catalysis. *EMBO J.* **34**, 2506–2521 (2015).
48. Seirafi, M., Kozlov, G. & Gehring, K. Parkin structure and function. *FEBS J.* **282**, 2076–2088 (2015).
49. Sarraf, S. A. et al. Landscape of the PARKIN-dependent ubiquitylome in response to mitochondrial depolarization. *Nature* **496**, 372–376 (2013).
50. Ziviani, E., Tao, R. N. & Whitworth, A. J. *Drosophila* Parkin requires PINK1 for mitochondrial translocation and ubiquitinates Mitofusin. *Proc. Natl Acad. Sci.* **107**, 5018–5023 (2010).
51. Gegg, M. E. et al. Mitofusin 1 and mitofusin 2 are ubiquitinated in a PINK1/parkin-dependent manner upon induction of mitophagy. *Hum. Mol. Genet* **19**, 4861–4870 (2010).
52. Tanaka, A. et al. Proteasome and p97 mediate mitophagy and degradation of mitofusins induced by Parkin. *J. Cell Biol.* **191**, 1367–1380 (2010).
53. Jin, S. M. & Youle, R. J. PINK1- and Parkin-mediated mitophagy at a glance. *J. Cell Sci.* **125**, 795–799 (2012).
54. McWilliams, T. G. et al. Basal Mitophagy Occurs Independently of PINK1 in Mouse Tissues of High Metabolic Demand. *Cell Metab.* **27**, 439–449.e5 (2018).
55. Peng, W., Schröder, L. F., Song, P., Wong, Y. C. & Krainc, D. Parkin regulates amino acid homeostasis at mitochondria-lysosome (M/L) contact sites in Parkinson's disease. *Sci. Adv.* **9**, eadh3347 (2023).
56. Alsina, D. et al. FBXL 4 deficiency increases mitochondrial removal by autophagy. *EMBO Mol. Med.* **12**, e11659 (2020).
57. Huemer, M. et al. Clinical, morphological, biochemical, imaging and outcome parameters in 21 individuals with mitochondrial maintenance defect related to FBXL4 mutations. *J. Inherit. Metab. Dis.* **38**, 905–914 (2015).
58. Gai, X. et al. Mutations in FBXL4, Encoding a Mitochondrial Protein, Cause Early-Onset Mitochondrial Encephalomyopathy. *Am. J. Hum. Genet.* **93**, 482–495 (2013).
59. Bonnen, P. E. et al. Mutations in FBXL4 Cause Mitochondrial Encephalopathy and a Disorder of Mitochondrial DNA Maintenance. *Am. J. Hum. Genet.* **93**, 471–481 (2013).
60. Cao, Y. et al. A mitochondrial SCF-FBXL$_4$ ubiquitin E3 ligase complex degrades BNIP$_3$ and NIX to restrain mitophagy and prevent mitochondrial disease. *EMBO J.* **42**, e113033 (2023).
61. Nguyen-Dien, G. T. et al. FBXL$_4$ suppresses mitophagy by restricting the accumulation of NIX and BNIP$_3$ mitophagy receptors. *EMBO J.* **42**, e112767 (2023).
62. Elcocks, H. et al. FBXL$_4$ ubiquitin ligase deficiency promotes mitophagy by elevating NIX levels. *EMBO J.* **42**, e112799 (2023).
63. Lee, J. J., Andreazza, S. & Whitworth, A. J. The STING pathway does not contribute to behavioural or mitochondrial phenotypes in Drosophila Pink1/parkin or mtDNA mutator models. *Sci. Rep.* **10**, 2693 (2020).
64. Moehlman, A. T., Kanfer, G. & Youle, R. J. Loss of STING in parkin mutant flies suppresses muscle defects and mitochondria damage. *PLoS Genet* **19**, e1010828 (2023).
65. Bravo, P. et al. Molecular characterization of PRKN structural variations identified through whole-genome sequencing. *Mol. Genet Genom. Med* **6**, 1243–1248 (2018).
66. Asakawa, S. et al. Analysis of eighteen deletion breakpoints in the parkin gene. *Biochem. Biophys. Res. Commun.* **389**, 181–186 (2009).
67. Mourier, A., Matic, S., Ruzzenente, B., Larsson, N.-G. & Milenkovic, D. The Respiratory Chain Supercomplex Organization Is Independent of COX7a2l Isoforms. *Cell Metab.* **20**, 1069–1075 (2014).
68. Wibom, R., Hagenfeldt, L. & von Döbeln, U. Measurement of ATP production and respiratory chain enzyme activities in mitochondria isolated from small muscle biopsy samples. *Anal. Biochem.* **311**, 139–151 (2002).
69. Filograna, R. et al. Modulation of mtDNA copy number ameliorates the pathological consequences of a heteroplasmic mtDNA mutation in the mouse. *Sci. Adv.* **5**, eaav9824 (2019).
70. Zeisel, A. et al. Cell types in the mouse cortex and hippocampus revealed by single-cell RNA-seq. *Science* **347**, 1138–1142 (2015).
71. Love, M. I., Huber, W. & Anders, S. Moderated estimation of fold change and dispersion for RNA-seq data with DESeq2. *Genome Biol.* **15**, 550 (2014).
72. Morbelli, S. et al. EANM practice guideline/SNMMI procedure standard for dopaminergic imaging in Parkinsonian syndromes 1.0. *Eur. J. Nucl. Med. Mol. Imaging* **47**, 1885–1912 (2020).
73. Stranneheim, H. et al. Integration of whole genome sequencing into a healthcare setting: high diagnostic rates across multiple clinical entities in 3219 rare disease patients. *Genome Med.* **13**, 40 (2021).
74. *Muscle Biopsy*. (Elsevier, 2021). https://doi.org/10.1016/C2016-0-00124-9.

Acknowledgements

The authors wish to thank Dr. Valina Dawson at Johns Hopkins University, who provided *Parkin*$^{loxP/loxP}$ mice. The authors wish to thank Fredrik Holmström and Linda Gillberg, (from Perlmann's lab, Karolinska Institutet) for the excellent technical assistance with tissue dissociation and FACS sorting. We thank Dr. Peter Zentis and Dr Astrid Schauss from the CECAD imaging facility for use of the microscopes and their help with the stereological analysis of TH positive neurons. This study was supported by grants to NGL from Vetenskapsrådet (2015-00418), Knut och Alice Wallenbergs Stiftelse, Hjärnfonden (FO2018-0151) and Parkinsonfonden. R.F. was supported by grants from Vetenskapsrådet (2022-01477), Loo och Hans Ostermans stiftelse, Åhlén-stiftelsen, KI Research Foundation Grants, StratNeuro and Hedlunds stiftelse. EM was funded by the Deutsche Forschungsgemeinschaft (SFB 1218—269925409 and EXC 2030—390661388). T.P. was supported by Knut och Alice Wallenbergs stiftelse and Vetenskapsrådet (VR 2020-00884). M.R. was financially supported by the Knut och Alice Wallenbergs Stiftelse as part of the National Bioinformatics Infrastructure Sweden at SciLifeLab. P.S. was supported by the Stockholm City Council and Knut och Alice Wallenbergs Stiftelse. Figures have been created using BioRender.com.

Author contributions

Conceptualization and design: R.F. and N-G.L.; Methodology: R.F., J.G., G.R., S.L. and K.T.; Investigation: R.F., J.G., H-N.C., G.R., M.B., M.O., S.L., M.R., R.W., S.R., I.N. and E.M.; Visualization: R.F. and E.M.; Funding acquisition: R.F., T.P., P.S., E.M. and N-G.L.; Project administration: R.F.,

C.K., T.P., A.Wr., A.We., P.S. and N-G.L.; Supervision: R.F. and N-G.L.; Writing: R.F. and N-G.L.; All authors read and approved the final manuscript.

Funding
Open access funding provided by Karolinska Institute.

Competing interests
N-G.L. is a scientific founder and owns stock in *Pretzel Therapeutics Inc* and declares no non-financial competing interests. R.F. and C.K. act as a paid consultant for *Pretzel Therapeutics Inc*. All other authors declare non. financial competing interests.

Additional information
Supplementary information The online version contains supplementary material available at https://doi.org/10.1038/s41531-024-00707-0.

Correspondence and requests for materials should be addressed to Roberta Filograna or Nils-Göran Larsson.